Direct and Sensitive Phase Readout for Integrated Waveguide Sensors

R. Halir
L. Vivien
X. Le Roux
D.-X. Xu
P. Cheben
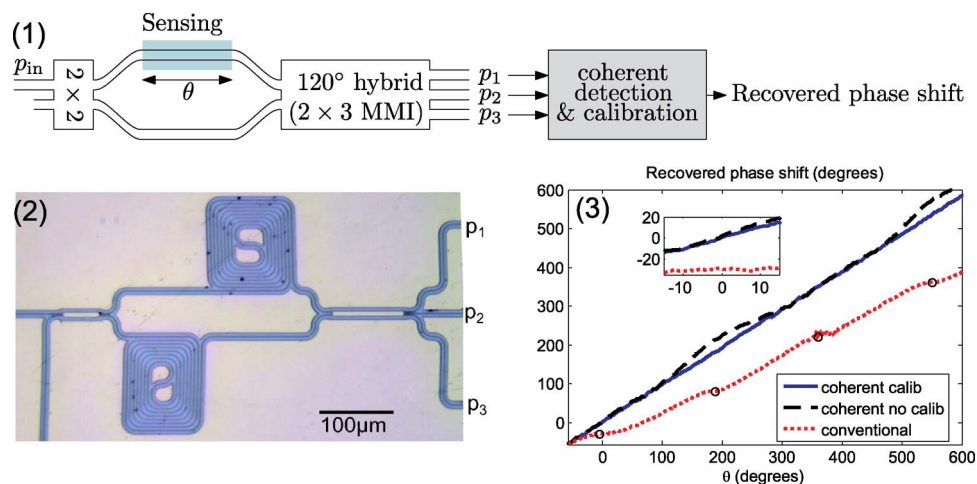
Direct and Sensitive Phase Readout for Integrated Waveguide Sensors

R. Halir, [1,2] **L. Vivien,** [3] **X. Le Roux,** [3] **D.-X. Xu,** [4] **and P. Cheben** [4]

[1] Departamento Ingeniería de Comunicaciones, ETSI Telecomunicación,
Universidad de Málaga, 29071 Málaga, Spain
[2] Bionand Center for Nanomedicine and Biotechnology, Parque Tecnológico de Andalucía,
29590 Málaga, Spain
[3] Institut d'Electronique Fondamentale, Université Paris-Sud, CNRS UMR 8622, 91405 Orsay, France
[4] National Research Council Canada, Ottawa, ON K1A 0R6, Canada

Abstract: Integrated optical affinity sensors based on Mach–Zehnder interferometers (MZIs) enable sensitive and label-free detection of chemical and biological molecules. However, since MZIs transduce optical phase changes into sinusoidal intensity variations, they exhibit a variable sensitivity that vanishes at the extrema of the transmittance function. Moreover, the direction of phase change cannot be unambiguously determined with these sensors. Here, we present a coherent detection scheme based on integrated optics that enables unambiguous readout of the optical phase with a constant sensitivity. Our approach furthermore cancels the effect of imperfections in the sensor hardware using a blind calibration scheme. We experimentally show completely linear readout of the optical phase, with a fourfold enhancement of average sensitivity compared to conventional detection.

Index Terms: Integrated optical sensors, phase detection.

1. Introduction

Integrated photonic waveguide sensors have demonstrated a strong potential for highly sensitive detection of chemical and biological molecules [1]. Being particularly amenable for multiplexed operation [2], [3], they have emerged as promising candidates for lab-on-a-chip devices. Several types of integrated optical sensors are commonly used, including ring resonators [4]–[6], bi-modal waveguides [7], and Mach–Zehnder interferometers (MZI) as shown in Fig. 1(a) [2], [8], [9]. The operation of these sensors is based on the interaction of the evanescent field of the waveguide mode with the analyte present on top of the waveguide, which induces a change in the effective index of the waveguide mode (Δn_{eff}). As the mode propagates along the sensing area of length L it acquires a phase shift

$$\theta = \frac{2\pi}{\lambda} \Delta n_{\text{eff}} L. \tag{1}$$

MZI sensors, which are widely used because of their simplicity, indirectly detect this phase shift by interferometrically converting it into an intensity modulation. However, the resulting sinusoidal output signal is not well suited for sensing, since the direction of phase change, corresponding to the adsorption and dissociation of the analyte, cannot be distinguished. Furthermore, the sensitivity of the sensor, $|dp_{\text{out}}/d\theta| \propto |\sin\theta|$, varies with θ, reaching a maximum in the region were the output is
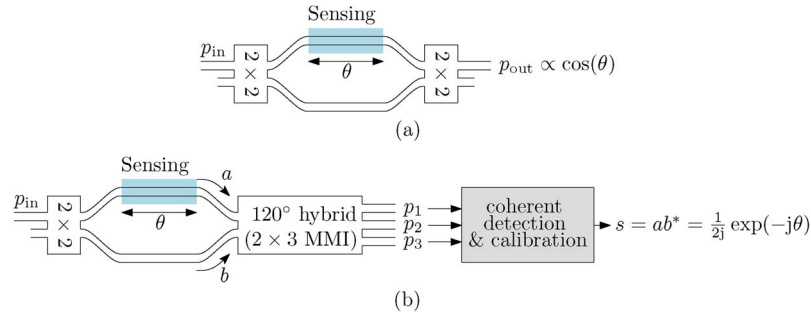
Fig. 1. (a) Schematic of a conventional MZI sensor and (b) a coherently detected MZI sensor with calibration to cancel hardware imperfections.

approximately linear, but vanishing near the extrema (maxima and minima). This limitation may be partially overcome by slightly modulating the wavelength of the input signal [10], which, however sacrifices some of the simplicity of the MZI structure. Alternatively, the use of a three-waveguide directional coupler at the MZI output was reported in [9], [11]. With this approach the three outputs are recorded simultaneously but are then treated independently: as θ varies, the output that offers the best sensitivity has to be selected, and the direction of phase change is manually inferred from the three outputs. Thus the application of this method can be rather challenging, especially when the variation of θ is rather complex.

Here, we propose a coherent detection scheme, that makes use of robust techniques developed for coherent optical communications. Our scheme uses a 120° hybrid, implemented with a 2×3 multimode interference coupler, at the MZI output [Fig. 1(b)]. By jointly processing the resulting output powers with coherent receiver techniques, we recover the complete amplitude and phase responses of the sensing element. Even intricate variations of θ are thus readily tracked. Our detection scheme furthermore enables blind calibration of the sensor hardware, so that θ is recovered correctly even in the presence of hardware imperfections. We experimentally show that our coherent detection scheme yields a linear response to the optical phase shift (1), and achieves a fourfold enhancement in the average detection limit compared to the conventional sensor. Near the transmittance extrema an order of magnitude enhancement is achieved.

2. Coherent Detection of the Sensor Response

In both the conventional sensor and our coherent approach, the input signal is equally split into the sensing arm and the reference arm [Fig. 1(a) and (b)]. The signal travelling through the reference arm can be expressed as $b = (j/\sqrt{2})\exp[-j2\pi n_{eff}L/\lambda]$, whereas the signal that has interacted with the analyte is $a = (1/\sqrt{2})\exp[-j2\pi(n_{eff} + \Delta n_{eff})L/\lambda]$, since it experiences an effective index change Δn_{eff}. In the coherent detection scheme, the 120° hybrid ideally combines the signal in the sensing arm, a, and the signal in the reference arm, b, with phase differences shifted by 120° at each output, yielding the output powers $p_1 = |(1/\sqrt{3})(a + b\exp(j2\pi/3))|^2$, $p_2 = |(1/\sqrt{3})(a + b)|^2$, and $p_3 = |(1/\sqrt{3})(a + b\exp(-j2\pi/3))|^2$. To extract θ from the output powers p_1, p_2, p_3 we proceed as follows. We compute a complex signal $s = x + jy$, with

$$x = p_2 - 0.5p_1 - 0.5p_3, \quad y = \frac{\sqrt{3}}{2}(p_1 - p_3). \tag{2}$$

As shown in [12], $s = ab^* = (1/2j)\exp(-j\theta)$, from which the phase shift θ is recovered as $\arg(s)$, i.e., the complex argument of s. Note that this detection scheme yields constant sensitivity, i.e., $|ds/d\theta| = (1/2)$, as opposed to the conventional scheme where sensitivity vanishes at extrema points. Since s furthermore identifies the quadrant in which θ lies, arbitrary variations of θ are unambiguously recovered (as long as there are no phase discontinuities larger than 360°).
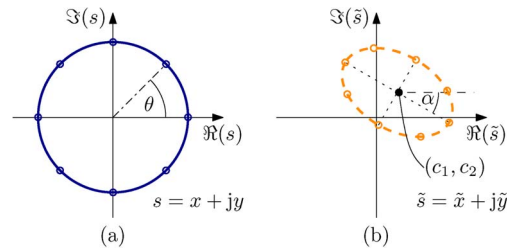
Fig. 2. Schematic representation in the complex plane of the detected signal, s, (a) in the ideal case, and (b) in the presence of hardware imperfections.

3. Calibration

The steps described in Section 2 to recover θ from p_1, p_2, p_3 assume ideal sensor hardware. However, two major impairments may arise in the measurement. First, due to fabrication variations the 120° hybrid will exhibit small deviations from the ideal 120° phase shifts. Second, the output powers (p_1, p_2, and p_3) may not be collected with the same efficiency. These deviations will result in errors in the recovered phase, as further discussed in Section 4. However, with our detection approach sensor hardware impairments can be cancelled using a blind calibration scheme, i.e., using only the measurement data, as described in the following. Under ideal conditions the output signal $s(\theta) = x + jy = (1/2j)\exp(-j\theta)$ describes a circle in the complex plane, centered at the origin, as shown schematically in Fig. 2(a). The aforementioned imperfections linearly transform the coordinates (x, y) into a new set of coordinates $(\tilde{x}, \tilde{y})$ [13]. Hence, the circle described by x and y will be mapped onto an off-center ellipse described by $\tilde{x}$ and $\tilde{y}$, as shown in Fig. 2(b). This mapping is independent of the phase shift that is sensed, thereby providing a straightforward procedure for sensor calibration from the raw measurement data: i) compute x and y using Eq. (2); ii) geometrically fit the points (x, y) to an ellipse, extracting the ellipse center, (c_1, c_2) and the angle of the major axis, α, as shown in Fig. 2(b); iii) use these parameters to move the data points to the origin, and scale them into a circle, yielding the calibrated signal s.

4. Experimental Results

To experimentally demonstrate that our coherent detection scheme can unambiguously recover the phase change (θ) with a constant sensitivity, both the conventionally detected MZI and a coherently detected MZI were implemented in the silicon-on-insulator (SOI) platform. Note that here we are interested in comparing two different types of circuits and their corresponding detection mechanisms, rather than studying the evanescent wave sensing of any particular chemical or biological species. Therefore, we implemented a path length difference ($\Delta L = 170$ μm) between the arms of both MZIs so that a phase difference $\theta = -(2\pi/\lambda_0^2)n_{\text{group}}\Delta L\Delta\lambda$ can be generated by scanning the input wavelength ($\Delta\lambda$), and in this way obviating the need for changing the cladding refractive index.

Both structures are realized on a 260 nm thick SOI substrate, use 450 nm wide interconnecting waveguides, and operate with transverse magnetic (TM) polarized light near $\lambda_0 = 1550$ nm. The 120° hybrid is implemented with a 2 × 3 MMI. While other devices, such as directional couplers [9] and adiabatic couplers [14] could also be used, MMIs are known exhibit a solid performance as optical hybrids [12], [15]. Using the design procedure described in [16], the dimensions of the fully etched 2 × 3 MMI were found to be 6.9 μm wide and 99.5 μm long. The waveguides are tapered to a width of 1.5 μm at the inputs and outputs of the MMIs to improve device performance. Our 3D full-vectorial simulations show that for TM polarization and at $\lambda_0 = 1550$ nm the 2 × 3 MMI exhibits an imbalance smaller than 0.1 dB and a deviation from the ideal 120° phase shifts between its outputs smaller than 0.3°. For variations of ± 0.1 μm in the width of the device, which is most critical dimensions, the imbalance is $\sim$1 dB and the phase error is $\sim$5°.

The MZI arms contain $\sim$4 mm long spiraled waveguides with the aforementioned 170 μm length difference. Surface grating couplers with subwavelength microstructures [17], [18], defined in the
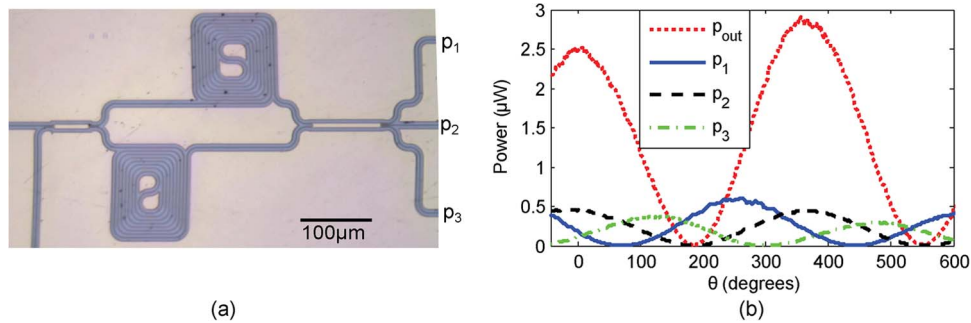
Fig. 3. (a) Optical microscope image of the coherently detected sensor. (b) Measured response of the output powers to a phase shift in one of the arms in the conventional device (p_{out}) and in the coherent sensor (p_1, p_2, p_3).

same etch step as the waveguides, are used for coupling light in and out of the chip. The couplers are arrayed with a pitch of 127 μm, so that light can be simultaneously coupled in and out with a single, angle-polished fiber array. The structures were defined using e-beam lithography, and transferred into the silicon with a single etch step using inductively coupled plasma-reactive ion etching (ICP-RIE). The chip was spin-coated with an SU-8 layer for protection. Fig. 3(a) shows a microscope image of the coherent sensor.

For characterization, the fiber array was aligned to each structure, and the output power was recorded as the input wavelength was scanned over ~5 nm to induce a phase shift (θ) between the arms. In the coherently detected sensor the three outputs (p_1, p_2, p_3) were recorded simultaneously. The unprocessed output powers are shown in Fig. 3(b). The average detected powers were 1.3 μW in the conventional sensor, and 0.7 μW in the coherently detected device, so that the overall signal to noise ratio in the unprocessed signals of both devices was similar. Imperfections resulting from fabrication variations are expected to be similar in both devices, since they are placed side by side on the chip. The actual phase shift (θ) shown in the x-axis of Fig. 3(b) is readily obtained from the positions of the extrema of the detected powers, and by taking into account that θ is directly proportional to the variation of input wavelength ($\Delta\lambda$), which is linear.

In the conventionally detected sensor, p_{out} was properly normalized and the recovered phase shift was obtained with an inverse cosine function [see Fig. 4(a)]. Note, however, that phase shifts beyond 180° cannot be unambiguously recovered from p_{out}, so that the result of the inverse cosine function has to modified every 180° by assuming that the recovered phase shift should be monotonic [the corresponding points are marked with circles in Fig. 4(a)]. It is furthermore observed that in these regions, which correspond to the maxima and minima of p_{out}, small changes in θ cannot be distinguished.

The three output powers of the coherently detected sensor (p_1, p_2, p_3) were processed as described above, yielding the complex signal s, from which the recovered phase shift was obtained as arg(s). Note that there are no phase ambiguities in this case since s uniquely identifies the quadrant in which θ lies. The effect of blind calibration on the recovered phase shift can be observed in Fig. 4(a): when hardware impairments are not corrected, the recovered phase shift is not linear, while after applying the blind calibration procedure a perfectly linear read-out of the phase shift is achieved. Furthermore, the coherently recovered phase exhibits an approximately constant sensitivity: small phase changes can be readily distinguished at any operation point.

For a quantitative comparison of the sensitivity of the coherent and conventional detection schemes, we compute the minimum detectable phase shift as follows. The recovered phase shifts shown in Fig. 4(a) are fitted piece-wise, over intervals of 15°, to straight lines. For each line the slope, d, is extracted. The standard deviation of the difference between the data and the fitted line represents the noise, σ_n, of the measurement. The minimum detectable phase shift, θ_{min}, was computed by requiring that the change in the signal be three times larger than the noise, i.e., $\theta_{min}\, d = 3\sigma_n$. Fig. 4(b) shows θ_{min} as a function of θ. As expected, the conventional sensors can
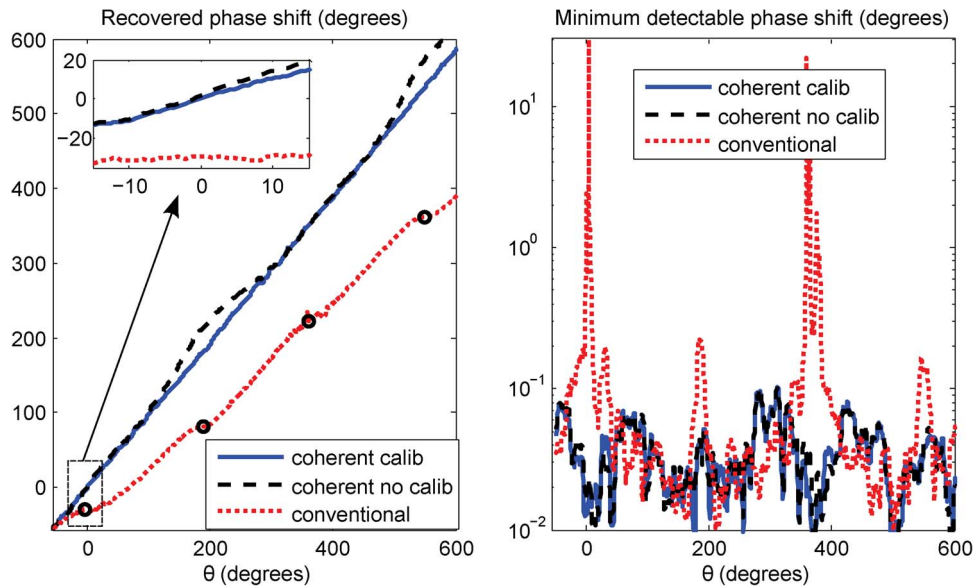
Fig. 4. (a) Recovered phase shift as obtained with conventional detection, coherent detection without calibration and coherent detection with calibration. The inset shows a detail of the recovered phase shift around $\theta = 0$. The circles denote points where the direction of phase change is ambiguous. (b) Minimum detectable phase shifts.

only detect larger phase changes ($\theta_{min} > 1°$) near the transmittance extrema. The coherently detected sensor exhibits a comparatively constant minimum detectable phase shift ($\theta_{min} < 0.1°$), showing an order of magnitude enhancement compared to the conventional sensor near the transmittance extrema, both with and without calibration. Averaging the minimum detectable phase shift over all values of θ yields $0.17°$ for the conventional scheme, and $0.04°$ for the coherent approach, i.e., more than a fourfold enhancement. The ripple in the minimum detectable phase shift is attributed to spurious reflections in the chip.

5. Conclusion

We have introduced the concept of coherent detection for photonic sensors. Our technique completely eliminates the regions of zero sensitivity in MZI based sensors, as well as the ambiguity in the sign of phase change, without requiring any wavelength tuning of the source. A blind calibration procedure that cancels hardware imperfections was developed, and a fourfold enhancement of sensitivity compared to conventional MZI sensors was experimentally achieved. These advantages of coherent detection techniques open excellent prospects for application in other sensor configurations that benefit from direct phase detection.

References

[1] X. Fan, I. White, S. Shopova, H. Zhu, J. Suter, and Y. Sun, "Sensitive optical biosensors for unlabeled targets: A review," *Anal. Chim. Acta*, vol. 620, no. 1, pp. 8–26, Jul. 2008.
[2] A. Densmore, M. Vachon, D. Xu, S. Janz, R. Ma, Y. Li, G. Lopinski, A. Delâge, J. Lapointe, C. Luebbert, Q. Y. Liu, P. Cheben, and J. H. Schmid, "Silicon photonic wire biosensor array for multiplexed real-time and label-free molecular detection," *Opt. Lett.*, vol. 34, no. 23, pp. 3598–3600, Dec. 2009.
[3] M. Iqbal, M. Gleeson, B. Spaugh, F. Tybor, W. Gunn, M. Hochberg, T. Baehr-Jones, R. Bailey, and L. Gunn, "Label-free biosensor arrays based on silicon ring resonators and high-speed optical scanning instrumentation," *IEEE J. Sel. Topics Quantum Electron.*, vol. 16, no. 3, pp. 654–661, May/Jun. 2010.
[4] D.-X. Xu, A. Densmore, A. Delâge, P. Waldron, R. McKinnon, S. Janz, J. Lapointe, G. Lopinski, T. Mischki, E. Post, P. Cheben, and J. H. Schmid, "Folded cavity SOI microring sensors for high sensitivity and real time measurement of biomolecular binding," *Opt. Exp.*, vol. 16, no. 19, pp. 15 137–15 148, Sep. 2008.

[5] W. Bogaerts, P. De Heyn, T. Van Vaerenbergh, K. De Vos, S. Kumar Selvaraja, T. Claes, P. Dumon, P. Bienstman, D. Van Thourhout, and R. Baets, "Silicon microring resonators," *Laser Photon. Rev.*, vol. 6, no. 1, pp. 47–73, Jan. 2012. [Online]. Available: http://dx.doi.org/10.1002/lpor.201100017

[6] C. Qiu, J. Chen, and Q. Xu, "Ultraprecise measurement of resonance shift for sensing applications," *Opt. Lett.*, vol. 37, no. 23, pp. 5012–5014, Dec. 2012. [Online]. Available: http://ol.osa.org/abstract.cfm?URI=ol-37-23-5012

[7] D. Duval, A. B. Gonzalez-Guerrero, S. Dante, J. Osmond, R. Monge, L. J. Fernandez, K. E. Zinoviev, C. Dominguez, and L. M. Lechuga, "Nanophotonic lab-on-a-chip platforms including novel bimodal interferometers, microfluidics and grating couplers," *Lab Chip*, vol. 12, no. 11, pp. 1987–1994, May 2012.

[8] R. Bruck, E. Melnik, P. Muellner, R. Hainberger, and M. Lämmerhofer, "Integrated polymer-based Mach-Zehnder interferometer label-free streptavidin biosensor compatible with injection molding," *Biosens. Bioelectron.*, vol. 26, no. 9, pp. 3832–3837, Mar. 2011.

[9] B. Drapp, J. Piehler, A. Brecht, G. Gauglitz, B. Luff, J. Wilkinson, and J. Ingenhoff, "Integrated optical Mach-Zehnder interferometers as simazine immunoprobes," *Sens. Actuators B, Chem.*, vol. 39, no. 1–3, pp. 277–282, Mar./Apr. 1997. [Online]. Available: http://www.sciencedirect.com/science/article/pii/S0925400597802183

[10] S. Dante, D. Duval, B. Sepúlveda, A. B. González-Guerrero, J. R. Sendra, and L. M. Lechuga, "All-optical phase modulation for integrated interferometric biosensors," *Opt. Exp.*, vol. 20, no. 7, pp. 7195–7205, Mar. 2012. [Online]. Available: http://www.opticsexpress.org/abstract.cfm?URI=oe-20-7-7195

[11] B. J. Luff, J. S. Wilkinson, J. Piehler, U. Hollenbach, J. Ingenhoff, and N. Fabricius, "Integrated optical Mach-Zehnder biosensor," *J. Lightw. Technol.*, vol. 16, no. 4, pp. 583–592, Apr. 1998.

[12] P. J. Reyes-Iglesias, I. Molina-Fernández, A. Moscoso-Mártir, and A. Ortega-Monux, "High-performance monolithically integrated 120° downconverter with relaxed hardware constraints," *Opt. Exp.*, vol. 20, no. 5, pp. 5725–5741, Feb. 2012. [Online]. Available: http://www.opticsexpress.org/abstract.cfm?URI=oe-20-5-5725

[13] A. Moscoso-Martir, I. Molina-Fernandez, and A. Ortega-Monux, "Signal constellation distortion and BER degradation due to hardware impairments in six-port receivers with analog I/Q generation," *Progr. Electromagn. Res.*, vol. 121, pp. 225–247, Dec. 2011.

[14] K. Solehmainen, M. Kapulainen, M. Harjanne, and T. Aalto, "Adiabatic and multimode interference couplers on silicon-on-insulator," *IEEE Photon. Technol. Lett.*, vol. 18, no. 21, pp. 2287–2289, Nov. 2006.

[15] R. Halir, G. Roelkens, A. Ortega-Moñux, and J. G. Wangüemert-Pérez, "High-performance 90° hybrid based on a silicon-on-insulator multimode interference coupler," *Opt. Lett.*, vol. 36, no. 2, pp. 178–180, Jan. 2011. [Online]. Available: http://ol.osa.org/abstract.cfm?URI=ol-36-2-178

[16] R. Halir, I. Molina-Fernández, A. Ortega-Monux, J. G. Wangüemert-Pérez, D.-X. Xu, P. Cheben, and S. Janz, "A design procedure for high performance, rib waveguide based multimode interference couplers in silicon-on-insulator," *J. Lightwave Technol.*, vol. 26, no. 16, pp. 2928–2936, Aug. 2008.

[17] R. Halir, P. Cheben, S. Janz, D.-X. Xu, I. Molina-Fernández, and J. G. Wangüemert-Pérez, "Waveguide grating coupler with subwavelength microstructures," *Opt. Lett.*, vol. 34, no. 9, pp. 1408–1410, May 2009.

[18] R. Halir, P. Cheben, J. H. Schmid, R. Ma, D. Bedard, S. Janz, D.-X. Xu, A. Densmore, J. Lapointe, and I. Molina-Fernández, "Continuously apodized fiber-to-chip surface grating coupler with refractive index engineered subwavelength structure," *Opt. Lett.*, vol. 35, no. 19, pp. 3243–3245, Oct. 2010.